Analysis of Ion Cyclotron Heating Issues for ITER

L.A. Berry 1), D.B. Batchelor 1), P.T. Bonoli 2), M.D. Carter 1), M. Choi 3),
W.A. Houlberg 1), D.A. D'Ippolito 4), R.W. Harvey 5), E.F. Jaeger 1), J.R. Myra 4),
H. Okuda 6), C.K. Phillips 6), E.J. Valeo 6), and J.C. Wright 2)

e-mail--**berryla@ornl.gov**

1) Oak Ridge National Laboratory*, Oak Ridge, TN 37831 (USA)
2) Plasma Science and Fusion Center, MIT, Cambridge, MA 02139 (USA)
3) General Atomics, San Diego, CA 92186 (USA)
4) Lodestar Research Corporation, Boulder, CO 80301 (USA)
5) CompX, Del Mar, CA 92014 (USA)
6) Princeton Plasma Physics Laboratory, Princeton, NJ 08543 (USA)

Abstract. Ion Cyclotron Resonance Heating (ICRH) is a major component of the planned heating systems for ITER. Twenty MW of RF power at 50 MHz is planned for initial operation with the possibility of an additional 20 MW for subsequent non-inductive modes of operation. Possible species mixes include dominantly H or D plasmas with a He-3 minority for initial operation, D-T with both thermal and fast-alpha populations for Q~10 inductive operation at relatively high density, and D-T with both thermal and fast alpha populations for non-inductive, Q~5 operation. Different ICRH modes are required to meet the requirements for these phases of operation, including minority and 2nd harmonic heating. RF-plasma interactions can include mode conversion, parasitic absorption on fast ion components, and energetic-ion tail formation. In order to contribute to the development and understanding of ICRH on ITER, we have begun analyzing the various options using the AORSA2D and TORIC full-wave simulation codes. In addition, we have computed quasi-linear diffusion operators from the AORSA2D RF fields that are input to the CQL3D Fokker-Planck code. When the RF-driven energetic tails are of sufficient density and/or energy to affect RF propagation and absorption, these distribution functions can be passed back to AORSA2D, allowing iteration to convergence. Our principal results, which are consistent with trends found previously with more approximate models, include: 1. At the higher range of densities (greater than 4-6 10^{19} m^{-3}) planned for Q~10 inductive operation, RF-tails from either minority heating or from RF absorption by fusion alphas are not significant. Lower densities and/or increased power will increase the possibilities of such tail formation. 2. For nominal Q~10 operation, absorption of the power by fusion alphas is in the 1-5% range of the total coupled RF power. We find the absorption by a non-Maxwellian slowing-down fusion-alpha distribution to be the same as a 1.2 MeV equivalent Maxwellian. 3. There is a Be resonance at the inner edge of the plasma (depending on details of magnetic field and wave frequency) that has the potential for unwanted edge absorption. 4. Mode conversion can be significant for densities in the 2–3 10^{19} m^{-3} range.

1. Introduction

Ion Cyclotron Resonance Heating (ICRH) at a frequency of 50 MHz and a power of 20 MW is planned for the Q ~ 10 initial phase of ITER operation and the Q ~ 5 extended pulse phase Substantial non-inductive current drive is required for the latter, and an additional 20 MW of ICRH power is possible. During the past several years there has been extensive development and benchmarking of the TORIC [1] and AORSA2D [2] full-wave ICRH codes. AORS2D can now calculate ICRH wave propagation and absorption for numerical, non-Maxwellian

distribution functions, and computes the quasi-linear operator necessary to evolve the distribution function using the CQL3D [3] bounce-averaged 3D Fokker-Planck code. AORSA2D and CQL3D can now iterate to a steady state on a single run. We have analyzed several ITER scenarios with these tools both to compare with earlier, less complete models and to use the new capabilities of these codes in order to begin understanding how to develop improved scenarios. In the remainder of this paper we present the results of the TORIC-AORSA2D benchmarking (Section 2); the development of non-Maxwellian energetic particle tails (Section 3), an analysis of a mode-conversion flow drive scenario (Section 4) and a brief summary (Section 5).

2. Benchmark Results

The parameters for the TORIC-AORSA2D comparison are presented in Table 1. Plasma species included T, D, He-4 (alpha ash), He-4 (energetic alphas), and Be.

TABLE 1 Q~10 Case with Second-Harmonic Tritium heating

Plasma Parameters	ICRF Parameters
$n_e(0) = 1.02\ 10^{20}\ m^{-3}$	f = 53 MHz
$T_e(0) = 24.8$ keV	$N_\varphi = 27$
$T_i(0) = 21.2$ keV	$P_{rf} = 20$ MW
$n_D : n_T = 31.6 : 50$	$H_{ant} = 1.76$ m
$n_{\alpha\_fast} / n_e = 0.76\%$ (on axis)	$R_{ant} = 8.165$ m
$n_{\alpha\_thermal} / n_e = 4.4\%$	$J_{ant}(\theta)$ = Gaussian
$n_{Be} / n_e = 2\%$	

Fields calculated by these codes, E_+ for TORIC and E_x (the component of perpendicular field most closely aligned with the major radius) for AORSA are shown in Figure 1.

While the plots appear different because of different color scale choices, the two calculations have the same qualitative behavior. The power is launched at the outer midplane from an antenna that has a height of almost two meters, and focuses as it propagates towards the magnetic axis. These results are compared quantitatively in Table 2.

Two cases are shown for AORSA2D. The first (middle column) is for a Maxwellian energetic alpha distribution with a temperature of 1.2 MeV. This temperature is determined by fitting a Maxwellian with the same density and energy as a slowing down distribution. The third column has a slowing-down distribution. For all cases the total energy deposition was normalized to 20 MW. The powers absorbed by the dominate species-T, D, and electrons-are shown in the first three rows. These values are in reasonable agreement between the two codes. However the low percentage species-Be, He-ash, and He- fast-α-have significant differences in absorbed powers, with AORSA systematically predicting higher heating powers. The reason(s) for these differences are not understood, but the EM field structure indicates somewhat weaker wave absorption for AORSA on the majority species than for TORIC, possibly leading to larger fields at the alpha and Be resonances. The Be absorption, which takes place at the inner edge of the plasma, is a particular concern because, if it is realistic, indicates the possibility of power deposition on a flux surface near the antenna and of increased power loading on bumper limiters and the antenna itself. The deposition on fast alphas is higher for the Maxwellian equivalent to a slowing down distribution and likely

results from absorption by the high energy tail from the Maxwellian. The 2nd harmonic T resonance is close to the magnetic axis.

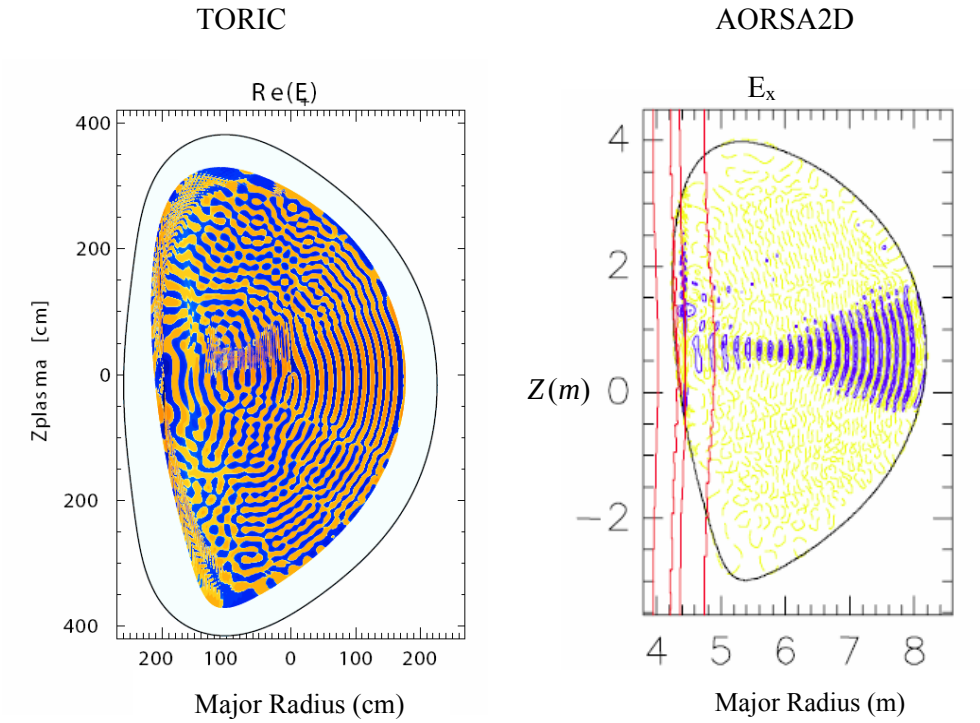

Figure 1. Comparison of perpendicular fields for 2nd harmonic T heating

TABLE 2 Q~10 Case with Second-Harmonic Tritium heating

Absorption (by species)	**TORIC (Maxwellian α's)**	**AORSA (Maxwellian α's)**	**AORSA (Slowing down α's)**
P(2Ω_T)	43.1 %	38.4 %	39.1 %
P(ELD)	50.4 %	45.6 %	47.0 %
P(D)	4.2 %	4.3 %	4.5 %
P(Be)	0.6 %	3.7 %	4.05 %
P(He-4)	0.41 %	2.8 %	3.0 %
P(fast-α)	0.90 %	5.1 %	2.3 %

2. Energetic Tail Formation

The possibility of the ICRC power coupling to the energetic fusion alpha population and then creating a tail with increased energy and greater ICRH absorption was examined using the coupled AORSA2D-CQL3D code suite for the nominal set of conditions described above. The results of this iteration are shown in Figure 2. The three sets of vertical panes present contour plots of the bounce-averaged distribution function as a function of parallel and perpendicular velocity and a log plot of this distribution function as a function of energy. These plots are typical of those at minor radii of 0.3~0.4, and are consistent with the relatively

broad radial profile of the alpha absorption. They show the development of the fast alpha distribution function as the RF produces a small tail. For this density, the increase in RF absorption by the alphas is small, and there is no runaway. The cause of the asymmetric tail is not understood, but may be due preferential interaction of fusion alphas moving in the same direction as the wave

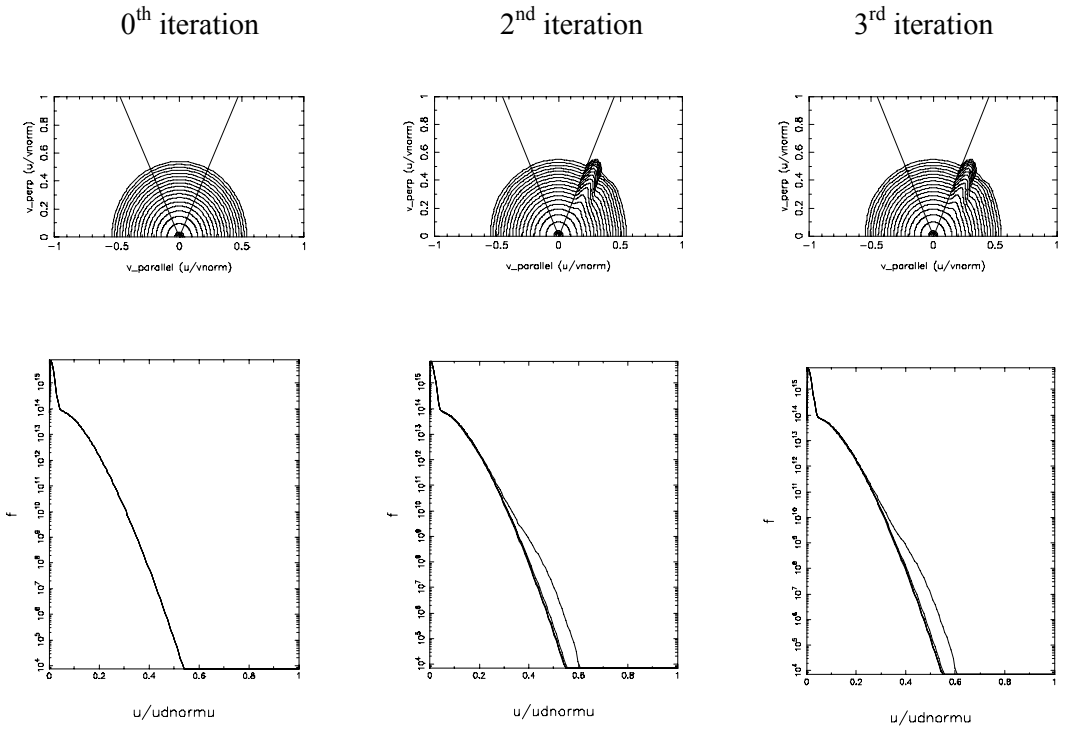

Figure 2. Self Consistent Tail Formation. The Oth,3rd, and 4th AORSA2D-CQL3D iterations showing the development of an small tail for an initial 1.2 MeV Maxwellian distribution.

We have also looked at T tail formation, and find that tritium tails do not form as a result of the RF heating for nominal T fractions. However, reducing the T density to 10% of the total does allow formation of a finite tail and a small increase of the T absorption from 6.8% (0th) to 7.7% (fourth iteration).

3. Mode Conversion and Flow Drive

Mode conversion scenarios offer the possibility of localized current drive and, speculatively, flow drive for turbulence suppression. We have examined a range of parameters for significant mode conversion using high-resolution AORS2DA simulations, and find that D-T-He^3 mixtures at somewhat reduced densities (such as might be used in non-inductive current drive scenarios) appear to offer the greatest potential. Figure 3 shows the results of a

simulation with D(20%):T(20%):He^3(30%) at a density of 2.5 10^{19} m^{-3}. This calculation had a resolution of 350x350 modes, and required about 6000 processor hours on the National Center for Computational Science Cray XT3 at Oak Ridge. The vertical lines show (right to left) the He^3 cyclotron frequency, ion-ion hybrid resonance, D cyclotron frequency, and Be cyclotron frequency. The perpendicular electric field (E alpha) contours (left) show the fast-wave mode structure. The short wavelength parallel electric field (right) on the low-field side of the ion-ion hybrid resonance is indicative of an ion cyclotron wave.

A detailed search of possible species mixtures has not been completed and it is possible that scenarios with more interesting densities and species mix may be found.

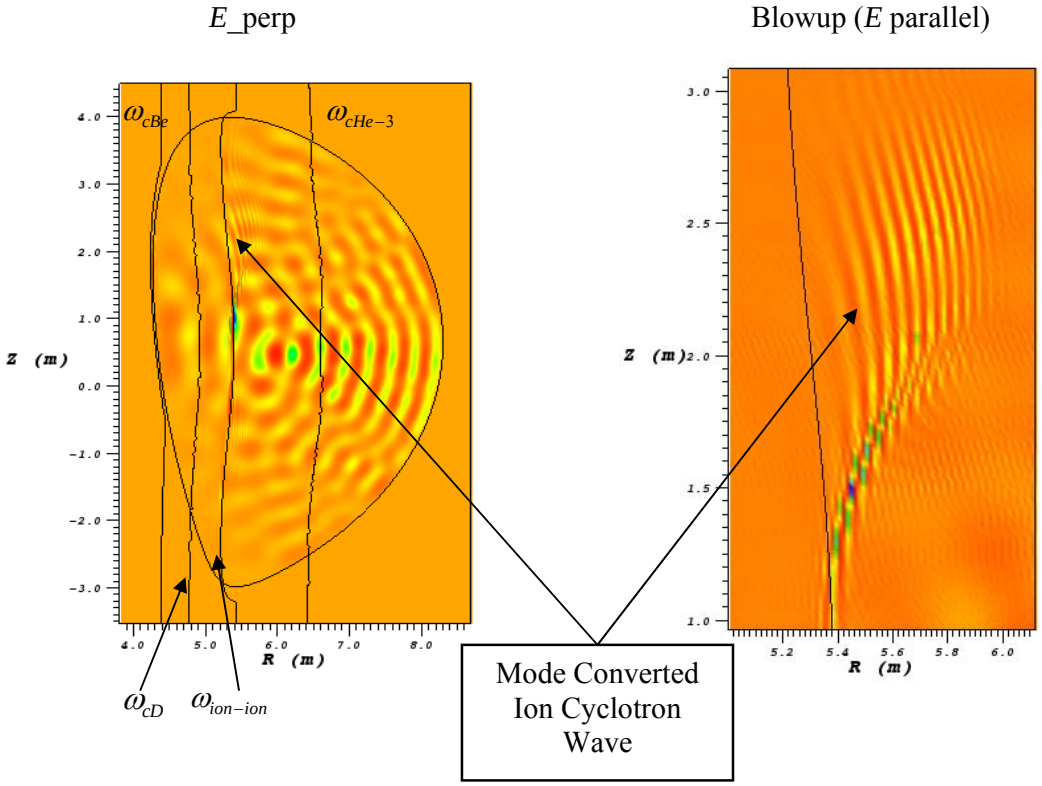

Figure 3. AORSA2D simulation of mode conversion in ITER. The vertical contours indicate

The RF fields both deposit momentum in the plasma, and, for the case of waves with significant kinetic flux, can transport momentum from one location in the plasma to another. The approach used calculating these RF driven forces and the resulting flows is based on [4] for calculating the RF forces and on [5, 6,7] for obtaining the resulting flows. The steady-state parallel, radial, and toroidal force/torque balance equations in combination with the constraint imposed by incompressible flow in a tokamak are utilized. Namely:

Parallel force balance: $\left\langle \vec{B}\cdot\vec{\nabla}\cdot\vec{\Pi}\right\rangle_{neo}+\left\langle \vec{B}\cdot\vec{\nabla}\cdot\vec{\Pi}\right\rangle_{anom}=\left\langle \vec{B}\cdot\vec{F}_{RF}\right\rangle$.

Radial force balance: $G=-\dfrac{-2\pi}{\psi'}\left[\dfrac{p'}{qn}+\phi'\right]$.

Toroidal torque balance: $\left\langle R\hat{\varphi}\cdot\vec{\nabla}\cdot\vec{\Pi}\right\rangle_{anom}=\left\langle \hat{\varphi}\cdot R\vec{F}_{RF}\right\rangle$.

Flow constraint: $\vec{V} = K\vec{B} + RG\hat{\varphi}$.

In these expressions the subscript "neo" refers to neoclassical viscous stress response and "anom" represents micro-turbulence induced transport responses. $\vec{F}_{RF}$ is the RF-induced force and $\langle ... \rangle$ indicates a flux surface average. The poloidal flux is indicated by ψ, $\rho(\psi)$ is a general radial coordinate, and "prime" indicates derivatives with respect to ρ. The quantities $p(\rho)$ (ion pressure), $n(\rho)$ (ion density), and $\phi(\rho)$ (plasma potential) are flux-surface functions. This is also the case for the toroidal rotation frequency, $G(\rho)$, and the parallel flow-constraint $K(\rho)$ (for simplicity, we *K* instead of the more general notation used in [6]). We have assumed a single ion species, neglected parallel heat fluxes, and have not included friction with the electrons. This formulation precludes dynamic interaction with turbulence induced stresses.

We will use the two in-surface force balance equations, parallel and toroidal, to obtain the plasma flow, and then can (although not presented in the paper) use that flow to determine the induced (incremental) radial electric field. The parallel neoclassical stress is assumed large compared to possible Reynolds stress contributions from micro-turbulence. However, the neglect of this stress in the parallel force balance may be questionable in light of the fine spatial structure possible with resonant RF absorption and, for the ITER analysis, relatively small values of the viscosity near the magnetic axis. We use that stress in the form $\left\langle \vec{B} \cdot \vec{\nabla} \cdot \vec{\vec{\Pi}} \right\rangle_{neo} = \mu \left\langle B^2 \right\rangle K$ where μ is the neoclassical viscosity to find $K = \dfrac{\left\langle \vec{B} \cdot \vec{F}_{RF} \right\rangle}{\mu \left\langle B^2 \right\rangle}$.

The anomalous toroidal torque viscosity is cast in the form:

$$\left\langle R\hat{\varphi} \cdot \vec{\nabla} \cdot \vec{\vec{\Pi}} \right\rangle_{anom} = \frac{1}{\rho V'} \frac{\partial}{\partial \rho} \left[\rho \left\langle \vec{\nabla} \rho^2 \right\rangle V' D \frac{\partial}{\partial \rho} \left\langle RV_t \right\rangle \right]$$

where *D* is an anomalous diffusion constant that is assumed proportional to the anomalous ion thermal conductivity [8]. No pinch term is included, but cannot be excluded. This leads to

$$\frac{1}{\rho V'} \frac{\partial}{\partial \rho} \left[\rho \left\langle \vec{\nabla} \rho^2 \right\rangle V' D \frac{\partial}{\partial \rho} \left\langle RV_t \right\rangle \right] = \left\langle \hat{\varphi} \cdot R\vec{F}_{RF} \right\rangle .$$

The solution for $\langle Rv_t \rangle$ can then equated to the toroidal projection of the flow constraint to obtain

$$G = \frac{1}{\left\langle R^2 \right\rangle} \left[\left\langle RV_t \right\rangle - KRB_t \right] .$$

The perpendicular force balance equation can then be then used obtain the radial derivative of the potential.

Figure 4 shows the results of RF force and flow velocity calculations for the mode-conversion case in Figure 3. For this case, even though there is significant mode conversion, power is concentrated near the plasma center in association with the 2nd harmonic tritium resonance. Because we are interested in bulk plasma flows, only the ions are of interest. The He-3 minority dominates the ICRH absorption by ions, and, as a result, the strongest force, is seen be associated with the He-3 minority. For this case, this allows force balance analysis with a single ion species. The resulting toroidal force is shown in Fig. 4a. Figures. 4b and 4c show the toroidal rotation, *G,* and parallel flow, *K,* response to this force. For this case, the two are

opposite in sign and nearly proportional. This indicates, as a result of the incompressible flow constraint, that the net toroidal torque is small compared to the poloidal RF force. The $\vec{E} \times \vec{B}$ shear obtained from the present solution is in the 10^5 s^{-1} range [9] that is thought to be significant for turbulence suppression, but may be an over estimate because not including anomalous diffusion in the parallel force balance.

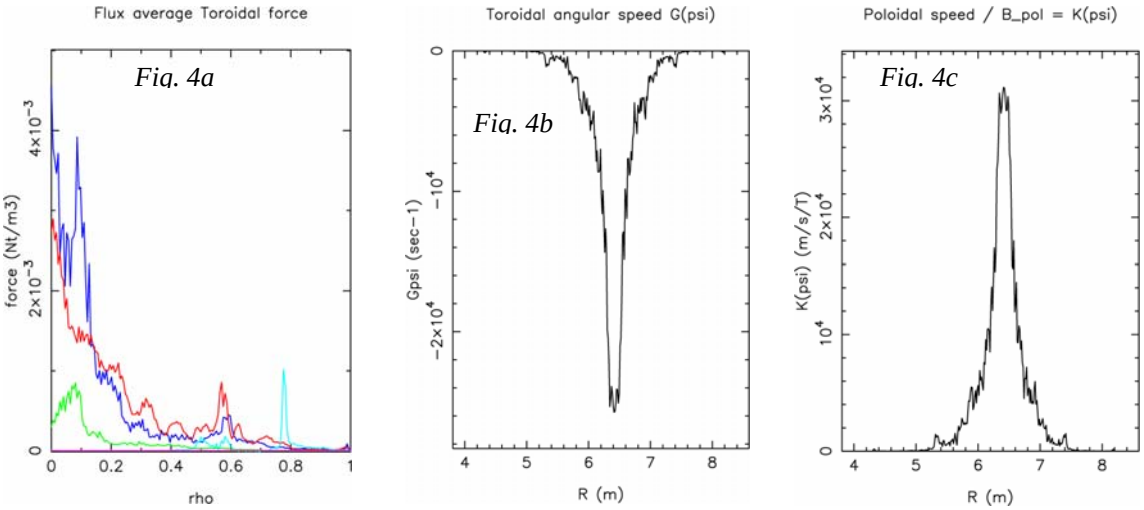

Figure 4. The flux-surface averaged toroidal force, toroidal angular speed (H-3) and poloidal velocity(He-3) for the ITER mode conversion case. The force is shown for He-3 (blue) electrons (red) T (green) and D (light blue)

5. Summary

We have begun a detailed examination of planned and potential uses of ICRH power in ITER. Over all our results are consistent with trends found previously with more approximate models. At the higher range of densities (greater than 4-6 10^{19} m^{-3}) planned for Q~10 inductive operation, RF-tails from either minority heating or from RF absorption by fusion alphas are not significant. Lower densities and/or increased power will increase the possibilities of such tail formation. For nominal Q ~ 10 operation, absorption of the power by fusion alphas is in the 1-5% range of the total coupled RF power. We find the absorption by a non-Maxwellian slowing-down fusion-alpha distribution to be the same as a 1.2 MeV equivalent Maxwellian. A potential issue is absorption by a Be resonance at the inner edge of the plasma (depending on details of magnetic field and wave frequency) that has the potential for unwanted edge absorption. Mode conversion can be significant for densities in the 2-3 10^{19} m^{-3} range. However, for ITER conditions, RF forces and resulting flows are mainly associated with the 2nd harmonic tritium resonance, and tend to be localized towards the plasma center. Flows driven by poloidal RF forces appear to be important, and lead to the need for more refined treatment of the parallel force balance when coupled with RF.

More detailed analyses to understand differences between AORSA2D and TORIC for RF absorption by slowing-down alphas, and the Be impurity are planned. In addition, further assessments will be made of how to use ICRH RF power to optimize ITER performance for both Q ~ 10 operation and for the extended pulse length Q ~ 5 operation with significant non-

inductive current drive. Finding higher density mode-conversion scenarios at lower He^3 densities is a particular issue for finding parameter ranges where flow stabilization might be observed.

*This work was supported by the offices of Fusion Energy Science and Advanced Scientific Computing Research in the U. S. DOE. Computer resources for this effort were, in part, provided by the National Center for Computational Sciences at Oak Ridge National Laboratory (ORNL). ORNL is managed by UT-Battelle, LLC, for the DOE under contract DE-AC05-00OR22725.

[1] BRAMBILLA, M., Plasma Phys. and Contr. Fusion **44**, 2423 (2002).
[2] JAEGER, E.F., BERRY, L.A., et al., Phys. Plasmas **13**, (2006).
[3] HARVEY, R.W. AND MCCOY, M.G., Proceedings of the IAEA Technical Committee Meeting on Advances in Simulation and Modeling of Thermonuclear Plasmas, Montreal, 1992, p. 489-526, IAEA, Vienna (1993).
[4] MYRA, J.R., BERRY, L.A., JAEGER, E.F., and D'IPPOLITO, D.A., Phys. Plasmas **11**, 1786 (2004).
[5] MYRA, J. R., and D'IPPOLITO, D. A., Phys. Plasmas **9**, 3867 (2002).
[6] HOULBERG W.A., SHAING, K.C, HIRSHMAN, S.P., ZARNSTORFF, M.C., Phys. Plasmas **4**, 3230 (1997).
[7] HIRSHMAN, S.P. and SIGMAR, D.J., Nucl. Fusion **21**, 1709 (1981).
[8] BURRELL, K.H. private communication.
[9] BURRELL, K.H., Phys. Plasmas 4, 1499 (1997).